Terr. Atmos. Ocean. Sci., Vol. 28, No. 6, 993-1008, December 2017 doi: 10.3319/TAO.2017.04.24.01

GPS TEC fluctuations over Tromsø, Norway, in the solar minimum

Wei-Sheng Chen[1], Chien-Chih Lee[1,*], Fang-Dar Chu[2], and Wai-Leong Teh[3]

[1] *General Education Center, Chien Hsin University of Science and Technology, Taoyuan City, Taiwan*
[2] *National Standard Time and Frequency Laboratory, Telecommunication Laboratories, Chunghwa Telecom Co. Ltd., Taiwan*
[3] *Space Science Centre, Institute of Climate Change, Universiti Kebangsaan Malaysia, Malaysia*

Article history:
Received 1 July 2016
Revised 18 April 2017
Accepted 24 April 2017

Keywords:
TEC fluctuations, Aurora, High-latitude irregularities

Citation:
Chen, W.-S., C.-C. Lee, F.-D. Chu, and W.-L. Teh, 2017: GPS TEC fluctuations over Tromsø, Norway, in the solar minimum. Terr. Atmos. Ocean. Sci., 28, 993-1008, doi: 10.3319/TAO.2017.04.24.01

ABSTRACT

This study investigated GPS TEC fluctuations over the high-latitude site, Tromsø, Norway (69.66°N, 18.94°E), in the solar minimum 2007 - 2008. The TEC fluctuation index Fp that defined by Mendillo et al. (Radio Science 2000) was adopted to quantify TEC fluctuations, in which $50 \le Fp < 200$ and $Fp \ge 200$ respectively represent moderate and strong irregularities. The investigations include the seasonal and temporal variation of Fp; the correlation between Fp and the magnetic indices Kp and AE; the comparisons between Fp and the ionospheric electron density observed by the Tromsø incoherent scatter radar and COSMIC. The results are that $Fp \ge 50$ occurred frequently in all seasons but $Fp \ge 200$ occurred more frequently in the equinoctial months; $Fp \ge 50$ mainly occurred in 18 - 04 LT, and maximized around 22 LT in the equinoctial months. The linear correlation between Fp and Kp was poor but that between Fp and AE was moderate. The maximal Fp and the percentages of $Fp \ge 50$ and $Fp \ge 200$ increased with Kp and AE; $Fp \ge 200$ is nearly negligible when $Kp < 4$. The high electron density structure that resulted from the auroral activity caused $Fp \ge 50$ when it located in the E region or extended from the E region to the F region. The findings are that $Fp \ge 50$ at auroral region mainly relates to the auroral activity. The Fp seasonal variation can be explained by the effect of sunlight and the geometry of the magnetotail. Occurrence of irregularities and their maximal intensity are increased with Kp and AE. Strong irregularities almost only occur in the magnetic disturbance period. Irregularities in the E region or in the E and F regions both can cause $Fp \ge 50$.

1. INTRODUCTION

The ionospheric irregularities is an active topic in the research of ionosphere and space weather because they can interfere with trans-ionospheric radio waves, which are the base of satellite communication. Various instruments and techniques have been used to explore irregularities, such as ionosonde, radar, rocket, and satellite communication. At high latitudes, because of the geomagnetic configuration, using radar to explore irregularities is not as effective as that at low latitudes. Therefore, the satellite communication is used more frequently. For exploring irregularities, there are two techniques based on satellite communication, which are scintillations and fluctuations of total electron content (TEC). In this study, the index derived from TEC fluctuations, which defined by Mendillo et al. (2000), was used to investigate irregularities over the high-latitude site, Tromsø, Norway.

The scintillation observation at high latitudes has been performed for many decades, and many papers were published. Contrarily, measuring TEC fluctuations becomes popular after Global Positioning System (GPS) deployment, and the number of the studies using TEC fluctuations is far less than using scintillations. Because scintillations have been investigated at Tromsø (Basu et al. 1988; Kersley et al. 1988), and the two techniques sense irregularities with different scale sizes, it is worth to see any difference between TEC fluctuations and scintillations at Tromsø to get more understanding about high-latitude irregularities.

A lot of knowledge about high-latitude irregularities come from scintillations. Early studies showed that scintillations are especially severe in the nightside auroral oval

* *Corresponding author*
E-mail: cclee@uch.edu.tw

and the dayside cusp region (Basu et al. 1988). Phase scintillations are more frequent and intense than amplitude scintillations (Hunsucker and Hargreaves 2003). Scintillations inside the auroral oval are usually a nighttime phenomenon but exist at all local time in the polar cap (Rino et al. 1983). The occurrence and intensity of scintillations increase strongly with the solar activity (Pryse et al. 1991). Numerous scientists have reported the variation of scintillations at the north European and American sites (e.g., Basu and Aarons 1980; Rino and Matthews 1980; Basu et al. 1988; Kersley et al. 1988, 1995; Prikryl et al. 2011; Jiao et al. 2013). The mechanisms for generating irregularities at high latitudes have been extensively reviewed by Tsunoda (1988) and Kelley (1989). Moreover, many papers (e.g., Prikryl et al. 2010, 2012; Shagimuratov et al. 2012) also contributed to the topic of high-latitude irregularities in various aspects.

Regarding TEC fluctuations, Wanninger (1993) first introduced the rate of TEC (ROT) for studying irregularities. Pi et al. (1997) subsequently defined a rate of TEC index (ROTI), the standard deviation of ROT at 5-min intervals, for studying the small-scale irregularities. The two papers both showed that TEC fluctuations occurred at high latitudes. Aarons (1997) used the parameter GPS phase fluctuations (the filtered ROT using a high pass filter) to study high-latitude irregularities. The author discovered that GPS phase fluctuations were activated when the site was in the auroral oval. Aarons and Lin (1999) and Aarons et al. (2000) further used GPS phase fluctuations to study irregularity development during magnetic storms. To characterize GPS phase fluctuations, Mendillo et al. (2000) defined the phase fluctuation index Fp to represent occurrence and strength of irregularities over a site. The index includes some advantages. First, the index captures both the spatially confined and stationwide/all-key pattern of TEC fluctuations in quantitative ways. Second, the index can be computed from the standard GPS observation data, which are public at the web site of International GNSS Service (IGS) and download freely. Finally, it is easy to implement the calculation procedure. This index has been applied to study irregularities at low and mid latitudes (Chen et al. 2006, 2011; Chu et al. 2008, 2009; Lee et al. 2009) but has not at high latitudes. Therefore, we adopted the Fp index in this study.

The intention of this study is to show a general picture of the Fp variation at high latitudes during the solar minimum. The investigation includes three parts. The first part shows the seasonal and temporal variation of Fp. The second part examines the correlation between Fp and the magnetic indices Kp and AE. In the third part, Fp is compared with ionospheric electron density observed the Tromsø UHF incoherent scatter radar (ISR) and Constellation Observing System for Meteorology, Ionosphere, and Climate (COSMIC) to get clues about the irregularity heights. This study is the extension of the brief report presented in 2016 Taiwan geosciences assembly (Chen et al. 2016). Because the amount of data in this study is far greater than that in the brief report, and more detailed investigations were also made. This study therefore is more complete and representative.

2. DATABASE

This study involves three kinds of data sets, which are the Fp index derived from the GPS data, the ionospheric electron density observed by Tromsø ISR, and the electron density profile from COSMIC.

The GPS data came from the TRO1 station (69.66°N, 18.94°E, MLAT 66.75°N, LT = UT + 1.26 hr), which is located at Tromsø, Norway. Figure 1 shows the location of the station and the trajectories of the ionospheric piercing points that are assumed to be at 350-km altitude. The data covered the two-year period from 2007 - 2008. The yearly average of sunspot numbers for the two years are 7.5 and 2.9, and 2008 is also marked as the solar minimum.

The raw GPS data contains the code and phase pseudoranges at frequencies 1575.42 and 1227.60 MHz. To get the Fp index, the 30-s vertical TEC (VTEC) was first calculated from these data (see Hofmann-Wellenhof et al. 1997 and Tiwari et al. 2013 for the details). To reduce the horizontal gradient of ionospheric electron density and the multipath effect, the VTEC with the elevation angles of satellites less than 15° were ignored. The time rates of VTEC (ROT) were then computed at 1-min intervals from the rest of VTEC.

$$\mathrm{ROT} = \left(\frac{\Delta \mathrm{VTEC}}{\Delta t}\right)_{\Delta t = 1\ \mathrm{min}} \tag{1}$$

A high pass filter was applied to further process ROT.

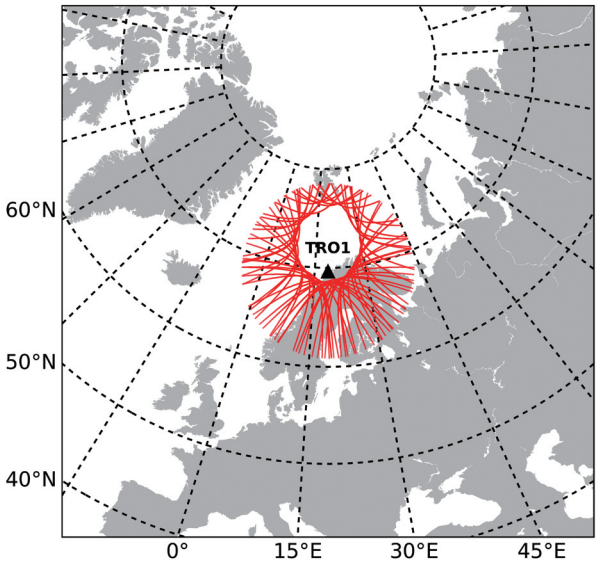

Fig. 1. The location of TRO1 GPS station and the trajectories of ionospheric piercing points (350 km). (Color online only)

The filter is a finite-impulse-response filter, which is designed using a 50-order Hamming window with the cutoff normalized frequency at 0.04 Hz. This filter can eliminate changes of ROT with the time scale higher than 25 min. Aarons et al. (1996) first referred to the output of the filter as GPS phase fluctuations, in which the word phase represents the phase pseudorange of the GPS data. However, the phrase, GPS phase fluctuations, may confuse with the phase changes of the GPS radio waves in the scintillation observation. To avoid misunderstanding, the output of the filter is referred to as FROT hereafter. (Similarly, the phase fluctuation index is referred to as the TEC fluctuation index.)

$$\mathrm{FROT} = \mathrm{High\ -\ Pass\ -\ Filter\ (ROT)} \tag{2}$$

Subsequently, the median of FROT (fp) was calculated every 15 minutes.

$$\mathrm{fp}(n, hr, i) = \mathrm{median}(|\mathrm{FROT}|) \tag{3}$$

where n is the satellite number; hr is the hour (00 - 23 UT); i is the 15-min time section within an hour ($i = 1, 2, 3, 4$).

Finally, an Fp index was obtained by averaging 15-min fp values in an hour.

$$\mathrm{Fp}(hr) = \frac{\sum_{n}^{nsat}\left\{\sum_{i}^{k}\left[\frac{\mathrm{fp}(n, hr, i)}{k}\right]\right\}}{nsat(hr)} \times 1000 \tag{4}$$

where $nsat$ is the total number of satellites observed within an hour; k is the number of fp available within each hour ($k = 1, 2, 3, 4$).

According to Mendillo et al. (2000), the magnitude of Fp can be divided into Fp < 50, 50 ≤ Fp < 200, and Fp ≥ 200 three levels, which represent the background noise, the moderate irregularities, and the strong irregularities, respectively. In this study, the level Fp ≥ 50 is also used to indicate irregularities either at the moderate level or at the strong level. It should be noted that the ROT is computed at 1-min intervals and the background plasma drift at high latitudes is typically about 1 km s^{-1}. Therefore, the scale size relates to Fp is around 60 km.

The ionospheric electron density was provided by the Tromsø ISR. This radar is a part of European Incoherent Scatter Scientific Association (EISCAT) radar system, which includes several transmitters and receivers in different locations. To get the electron density over Tromsø, the observations that the UHF transmitter and the receiver both locate at Tromsø were used. Moreover, the radar was operated in the aurora mode, in which the radar beam is fixed in the direction with a small tilt to the overhead (along the magnetic field line).

The electron density profile came from COSMIC. COSMIC is a satellite constellation system, which uses the radio occultation (RO) to explore the ionosphere. The whole system consists of six micro-satellites. Cooperating with GPS, it can provide more than 1000 globally distributed electron density profiles a day (Lei et al. 2007). According to the RO theory, the height of each element in a vertical profile is defined by the height of the tangent point of a radio path. Therefore, the COSMIC profile is not the vertical variation of electron density at a fixed location but the variation along a line in three-dimensional space (see Schreiner et al. 1999 for more details).

3. RESULTS

3.1 The Seasonal and Temporal Variations of Fp

Figure 2 shows the monthly occurrence rates of Fp for the dayside (06 - 18 LT) and nightside (18 - 06 LT) sectors. The rate is calculated from that, for a giving condition (a sector and a Fp level), the number of days met the condition in

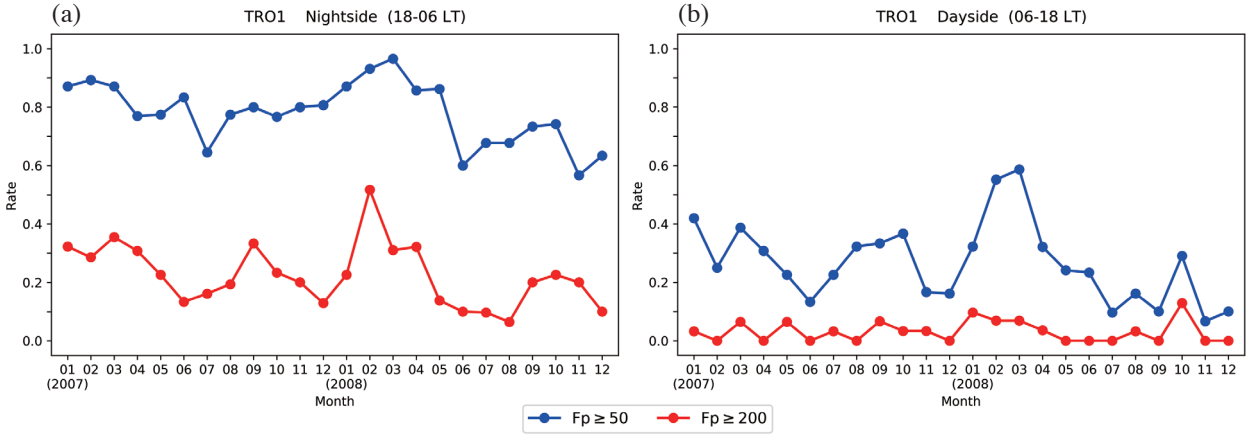

Fig. 2. The monthly occurrence rates of Fp for (a) the nightside sector (18 - 06 LT) and (b) the dayside sector (06 - 18 LT). (Color online only)

a month is divided by the total number of days in that month, in which a day met the condition indicates that day having at least one Fp in the giving sector and Fp level. For the nightside sector, the rates of Fp ≥ 50 all are higher than 0.5. On closer inspection, the rates of 2007 all are over 0.8 except July. In 2008, the rates of first five months uplift to higher levels, but the remainder drop to lower levels. Regarding Fp ≥ 200, peaks are located in the equinoctial months (March, April, September, and October, hereafter refer to as the E-months), and troughs are located in summer (May, June, July, and August, hereafter refer to as the J-months) and winter (January, February, November, and December, hereafter refer to as the D-months). For the dayside sector, most rates of Fp ≥ 50 and Fp ≥ 200 are lower than 0.4 and 0.1, respectively. The patterns of the two Fp levels are irregular as compared with that for the nightside sector. In addition, notable peaks of Fp ≥ 50 are located in the E-months.

Figure 3 shows the hourly occurrence rates of Fp. The rate is the number of Fp for a Fp level in an hour in a month divided the total number of Fp in that hour and that month. For Fp ≥ 50, most occurrences are in the period of 18 - 04 LT, and the maxima are around 22 LT in the E-months. In addition, November 2007 also has a notable maximum. The durations of Fp ≥ 50 in the E-months are longer than that in the D- and J-months. Particularly, June and July have the shortest duration and the latest starting time. For Fp ≥ 200, most occurrences are in the period of 18 - 02 LT. All Fp ≥ 200 rates are very low (< 0.3) and mainly distribute in the E-months. February 2008 has a notable maximum at 21 LT.

3.2 Fp and Magnetic Indices

Figure 4 is the scatter plots of Fp (≥ 50) against Kp for the dayside and nightside sectors, and the results of regression analysis. The figure shows that the maximal Fp increases with Kp, but the minimal Fp does not. The correlation coefficients are 0.475 for the nightside sector and 0.385 for the dayside sector. Because the coefficients both are lower than 0.5, the linear correlation between Fp and Kp is poor.

Figure 5 shows the percentages for different Fp levels at all Kp levels. The percentage for each Kp level is the number of Fp for a Fp level divided the total number of Fp. For the nightside sector, Fp ≥ 50 gradually increases since Kp = 0. It surpasses Fp < 50 at Kp = 2+ and then achieves saturation at Kp = 4. The increasing fo Fp ≥ 200 is more slowly, which becomes notable when Kp = 4-. For the dayside sector, Fp ≥ 50 gradually increases since Kp = 2 and surpasses Fp < 50 at Kp = 4. For Fp ≥ 200, it mainly distributes in the range Kp > 4. The characteristics of this figure are that the percentages of Fp ≥ 50 and Fp ≥ 200 both increase with Kp. Fp ≥ 50 becomes dominant when Kp > 2 for the nightside sector and Kp > 4 for the dayside sector. Fp ≥ 200 is far less than Fp ≥ 50 and nearly negligible when Kp < 4.

Figure 6 is the scatter plots of Fp (≥ 50) against AE for the dayside and nightside sectors, and the results of regression analysis. For the dayside sector, the trend that the maximal Fp increases with AE is clear. For the nightside sector, Fp and AE seem to reveal linear correlation when AE > 400. The correlation coefficients for the nightside and dayside sectors are 0.554 and 0.538, respectively. These values are higher than that between Fp and Kp and indicate the linear correlation between Fp and AE is moderate.

Figure 7 shows the percentages for different Fp levels at different AE levels. Each AE level is defined with a range of 100 (nT). The percentage at a AE level is the number of Fp for a Fp level divided the total number of Fp. For the nightside sector, Fp ≥ 50 increases markedly and becomes saturated at the level 500 - 600. Fp ≥ 200 increases slowly and steadily. For the dayside sector, Fp ≥ 50 gradually increases, which surpasses Fp < 50 at the level 500 - 600. Fp ≥ 200 starts increasing at the level 600 - 700. These results indicate that the percentages of Fp ≥ 50 and Fp ≥ 200 both increase with AE, and Fp ≥ 50 becomes dominant beyond the level 100 - 200 for the nightside sector and the level 500 - 600 for the dayside sector.

3.3 Fp and Ionospheric Electron Density

In 2007, there are 43 cases of the Tromsø ISR observations. Each case was compared with corresponding FROT and Fp. Figure 8 shows the case of 2007-01-20, which plots raw electron density (without calibration), FROT, and Fp during 18 - 24 UT. In this period, Kp varied from 2- to 2+; therefore, the observation was not conducted during the magnetic storm. The electron density was quite low in the first two hours. FROT showed no obvious activity, and thus the Fp values were less than 50. After 20 UT, an enhanced density structure occurred in the E region. An half hour later, the structure extended to the F region (about 250 km) and then lasted for 30 minutes. The structure finally split into the higher and lower two parts. The higher part vanished after 22 UT. The lower part, however, remained until the observation stop. FROT started to activate when the structure occurred, and then became highly activity when the structure extended from the E region to the F region. Meanwhile, the Fp values rose to the moderate level. After 22 UT, FROT showed slight activity and the Fp values also dropped to the background level. The average electron density of the structure was about 10^{11} m^{-3}. During 2130 - 2145 UT and 2220 - 2245 UT, the electron density around 100-km height was suddenly enhanced to 5×10^{11} m^{-3}, and FROT showed spikes.

Figure 9 shows another case, which was on 2007-01-19, and Kp varied from 2 - 3. The high electron density structure occurred at all times. During 19 - 24 UT, FROT was active and the Fp values were larger than 50. In the period of 20 - 21 UT, the electron density structure was very intense but mainly located in the E region. FROT in this

period still remained active and the Fp value was larger than 50. After all cases were examined, we found that FROT mainly responds with the structure which density is larger than 10^{11} m^{-3}. Moreover, the Fp value is higher than 50 when the high electron density structure occurs in the E region or extends from the E region to the F region.

To get more details about irregularities when Fp ≥ 50, the COSMIC profils around Tromsø in 2007 were examined. Figure 10 shows the COSMIC profile at 2036 UT on 2007-04-24. In Fig. 10a, Tromsø is marked as the black triangle. The red line represents the ground projection of the tangent points of the profile. The blue spot denotes the location of the maximal electron density of the profile. The green circle, which centers at Tromsø and has a 3° radius, indicates the region of interest. In Fig. 10b, the electron density profile is drawn as the red line. The blue spot marks the maximal electron density. The green shade represents the tangent points that are inside the green circle in Fig. 10a. Figure 10c shows the Fp variation, in which the arrow points to the time of the profile. The COSMIC electron density profile is derived

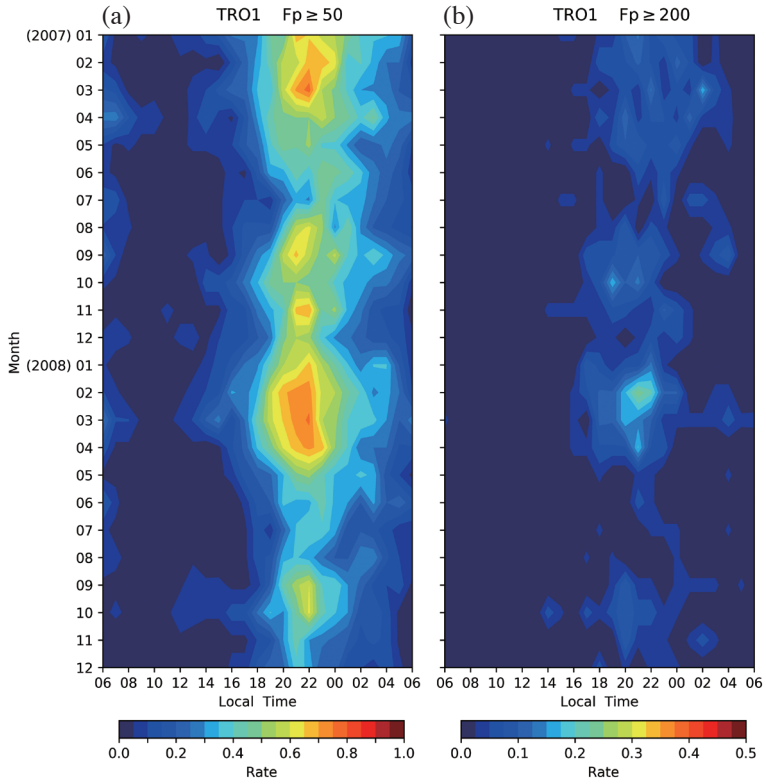

Fig. 3. The hourly occurrence rates of (a) Fp ≥ 50 and (b) Fp ≥ 200. (Color online only)

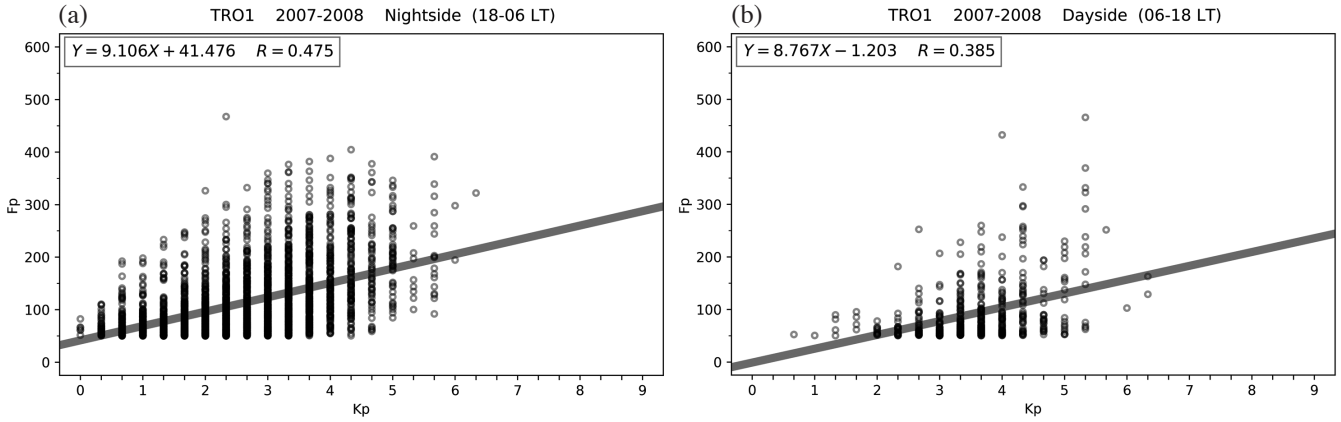

Fig. 4. The scatter plots of Fp against Kp for (a) the nightside sector (18 - 06 LT) and (b) the dayside sector (06 - 18 LT). The equation is the result of regression analysis. The R is the correlation coefficient.

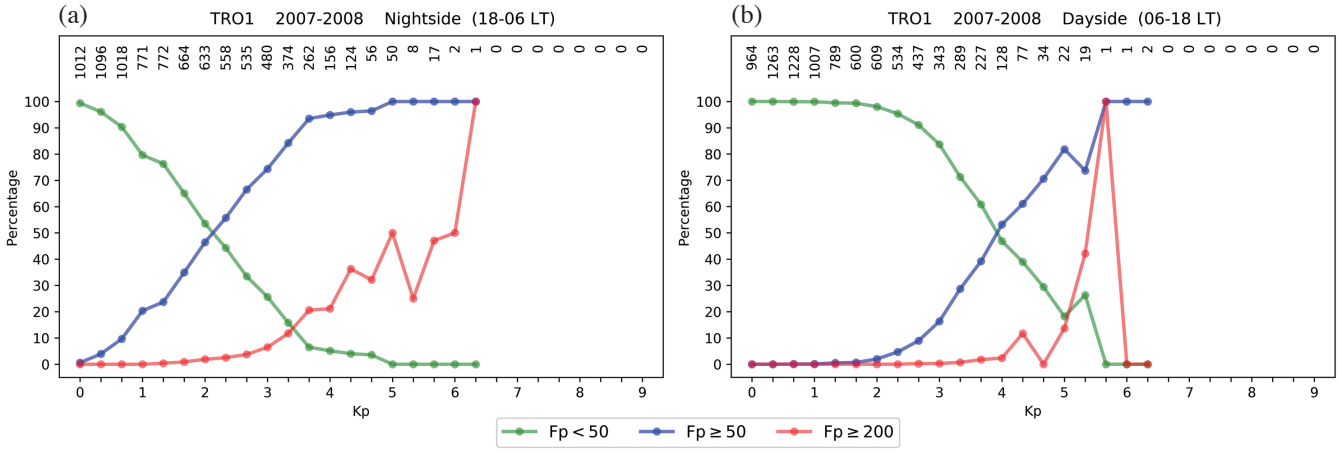

Fig. 5. The percentages of different Fp levels at all Kp levels for (a) the nightside sector (18 - 06 LT) and (b) the dayside sector (06 - 18 LT). The numbers on the top are the total number of Fp at every Kp level. (Color online only)

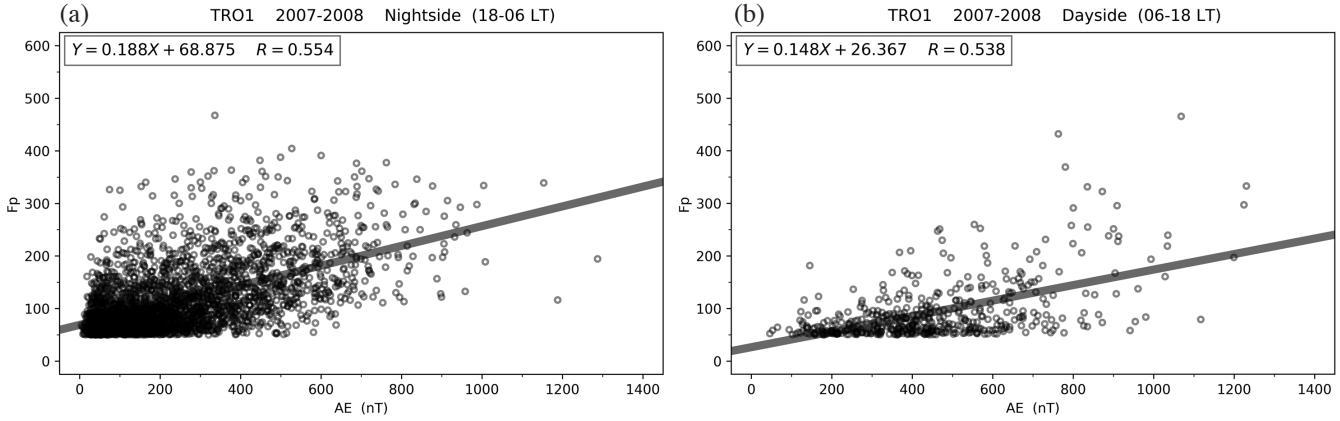

Fig. 6. The scatter plots of Fp against AE for (a) the nightside sector (18 - 06 LT) and (b) the dayside sector (06 - 18 LT). The equation is the result of regression analysis. The R is the correlation coefficient.

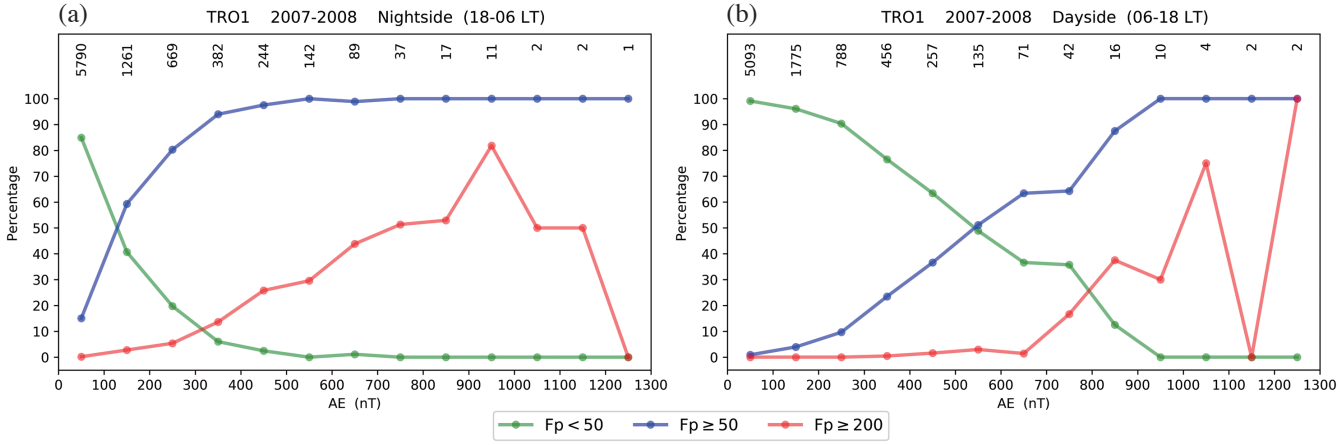

Fig. 7. The percentages of different Fp levels at different AE levels for (a) the nightside sector (18 - 06 LT) and (b) the dayside sector (06 - 18 LT). Each AE level is defined with a range of 100 (nT). The numbers on the top are the total number of Fp at every AE level. (Color online only)

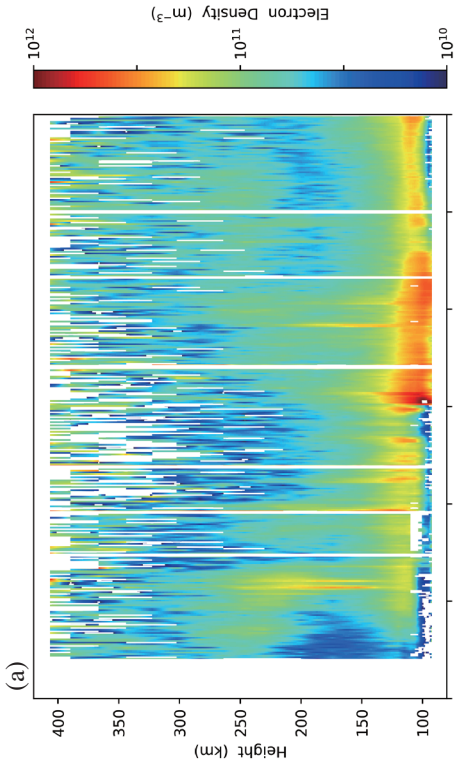

Fig. 9. The variations of (a) raw electron density (without calibration) observed by Tromsø UHF ISR, (b) FROT, and (c) Fp during 18 - 24 UT on 2007-01-19. In (b), different colors represent data from different satellites. (Color online only)

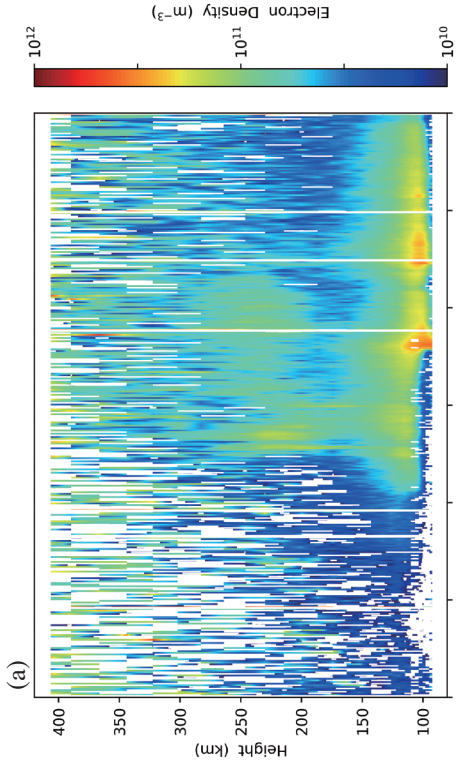

Fig. 8. The variations of (a) raw electron density (without calibration) observed by Tromsø UHF ISR, (b) FROT, and (c) Fp during 18 - 24 UT on 2007-01-20. In (b), different colors represent data from different satellites. (Color online only)

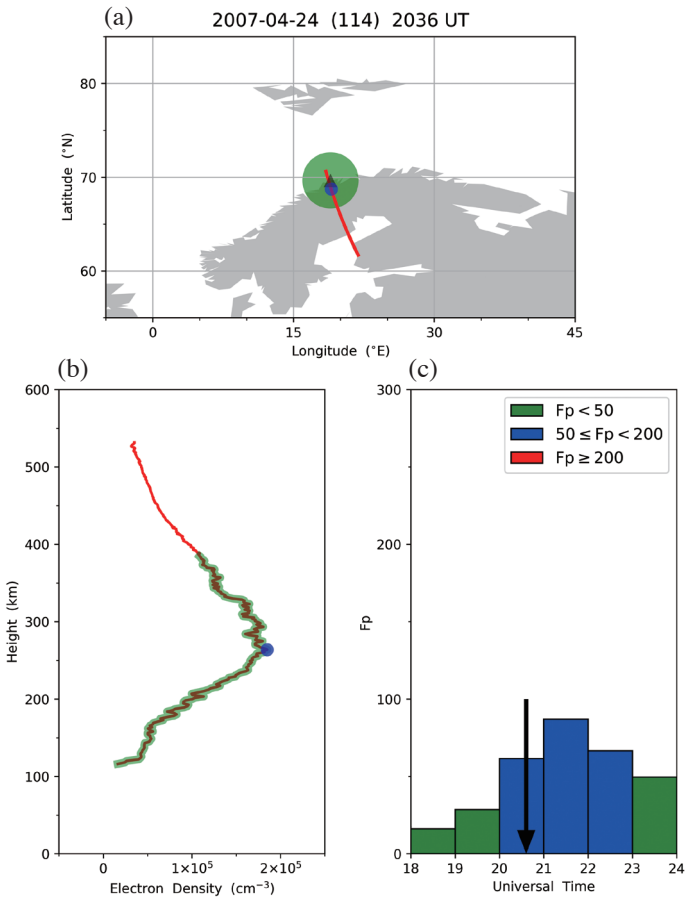

Fig. 10. (a) The ground projection of tangent points of the COSMIC electron density profile at 2036 UT on 2007-04-24. (b) The electron density profile. (c) The Fp variation. In (a), the black triangle marks the location of Tromsø. The red line is the ground projection of tangent points. The blue spot marks the location of the maximal electron density. The green circle, which centers at Tromsø and has the 3° radius, indicates the region of interest. In (b), the red line is the electron density profile. The blue spot marks the position of the maximal density. The green shade represents the tangent points inside the green circle in (a). In (c), the arrow points to the time of the profile. (Color online only)

using the Abel inversion. This method relies on a few assumptions and approximations (Lei et al. 2007), which often introduce errors in determining the profile. Errors are significant at lower altitudes or when the horizontal gradient of electron density is large. To suppress errors, we thus restricted our data to those with tangent points at main ionospheric altitudes (85 - 400 km) lying within the circle of interest. This approach makes the COSMIC profile close to the actual one. In the figure, the profile has sawtooth-like variations in the E and F regions. Meanwhile, the Fp value is larger than 50. Figure 11 shows another profile at 1935 UT on 2007-01-15. In the figure, the profile has great variations at about 100 km height. The Fp value is also larger than 50. These two cases indicate that irregularities in the E region or in the E and F regions both relate to Fp ≥ 50.

4. DISCUSSIONS

4.1 The Sources of TEC Fluctuations

Aarons (1997) has shown an example that, during the magnetic quiet time, the fluctuated FROT was observed over Tromsø when the site was inside the auroral oval. In this study, Fp ≥ 50 occurred almost every night and mainly distributed in the 18 - 04 LT period. Using the International Geomagnetic Reference Field (IGRF) (International Association of Geomagnetism and Aeronomy 2010) model and the auroral oval model (Feldstein 1963; Holzworth and Meng 1975), Fig. 12 shows the auroral oval during the magnetic quiet condition (Q = 3) and the track of Tromsø at the magnetic coordinates. Tromsø enters the oval at 1959 LT and leaves at 0300 LT. This period is just inside the period that Fp ≥ 50 frequently occurred. Therefore, Fp ≥ 50 is mainly related to the auroral activity. Another evidence is provided by Fig. 8 and the aurora observation at Kiruna, Sweden (67.8°N, 20.4°E, MLAT 64.44°N). According to the images of the all-sky camera at Kiruna in the same night (which are not shown in here), the luminous aurora occurred in the north margin of camera's field-of-view (which covered the sky of Tromsø) since 2018 UT. The aurora became vivid from 2025 - 2106 UT and then dimmed. The aurora

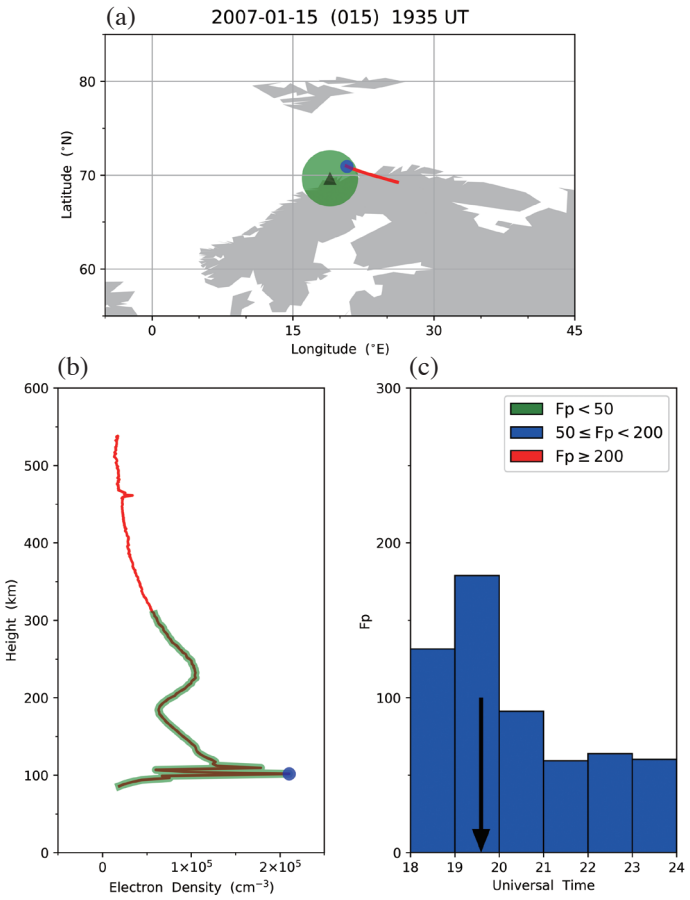

Fig. 11. (a) The ground projection of tangent points of the COSMIC electron density profile at 1935 UT on 2007-01-15. (b) The electron density profile. (c) The Fp variation. In (a), the black triangle marks the location of Tromsø. The red line is the ground projection of tangent points. The blue spot marks the location of the maximal electron density. The green circle, which centers at Tromsø and has the 3° radius, indicates the region of interest. In (b), the red line is the electron density profile. The blue spot marks the position of the maximal density. The green shade represents the tangent points inside the green circle in (a). In (c), the arrow points to the time of the profile. (Color online only)

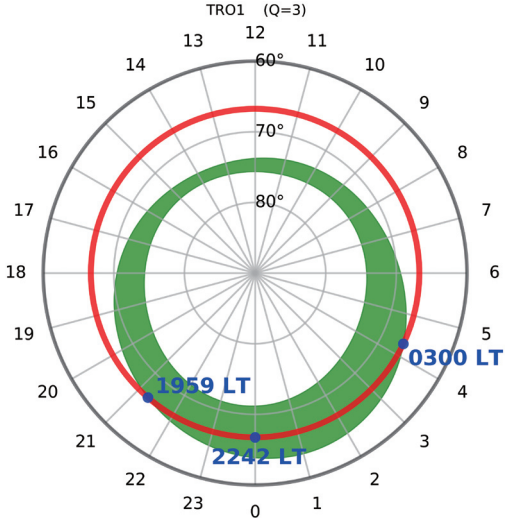

Fig. 12. The track of Tromsø and the auroral oval in the magnetic coordinates. The angular axis represents the magnetic local time (MLT). The radial axis represents the magnetic latitude (MLAT). The red line is the track of Tromsø, which orbits counterclockwise. The green area is the auroral oval during the magnetic quiet condition (Q = 3). The blue labels mark the time that Tromsø enters the oval, reaches the magnetic midnight, and exits the oval. (Color online only)

re-brightened at 2131 and 2217 UT, but the brightness lasted only a few minutes. Subsequently, the aurora appeared sporadically and faintly. Because the auroral activity is consistent with the electron density variation in Fig. 8, the high electron density structure should result from aurora and relate to Fp ≥ 50.

It is known that the aurora results from particle precipitation, which causes not only the luminous aurora but also ionization, heating, and magnetic disturbances. Through ionization, high electron density structures can emerge in a short period. Tsunoda (1988) showed (their Fig. 20) that, when the Chatanika ISR was used to observe particle precipitation, ionization structures were formed within 10 minutes and occupied altitudes between 100 and 300 km. Because those structures were irregular in space and time, which can be construed as a source of TEC fluctuations. Kelley et al. (1982) also suggested that particle precipitation is a crucial source of irregularities in the high-latitude ionosphere. In addition to particle precipitation, instability processes may also contribute to the generation of irregularities (Keskinen and Ossakow 1983; Tsunoda 1988). Kelley (1989) discussed the growth rate of the generalized E × B instability and the current convective instability, which create irregularities in the range from 0.1 - 30 km. However, the author concluded that the generalized E × B instability may be less dominant in the auroral zone, and the current convective instability can only rarely overcome the stabilizing effects of an unfavorable E × B geometry. Therefore, instability processes are not important as particle precipitation, especially for kilometer scale irregularities.

In the dayside sector, Tromsø was out of the auroral oval but Fp ≥ 50 still occurred. One possibility is that the ionospheric piercing points distribute in a large area. The GPS signals may penetrate the auroral oval and then Fp ≥ 50 occurs. Another possibility is the outer precipitation zone, which was discovered by Hartz and Brice (1967). This outer precipitation zone surrounds the auroral oval and covers the latitudes from 60 - 70°. In the dayside sector, the zone is located at latitudes lower than that of the auroral oval, but overlaps with the auroral oval in the nightside sector (Hunsucker and Hargreaves 2003). The precipitated particles in this zone are more energetic, and the ionization can be generated at even lower altitudes.

4.2 TEC Fluctuations and the Magnetic Activity

From Figs. 4 and 6, the linear correlation between Fp and Kp is poor, but that between Fp and AE has improvement, especially in the nightside sector when AE > 400. The Kp index is impacted by the ring current and more suitable for mid-latitude or global phenomena. Thus, the poor linear correlation between Fp and Kp is logical. The AE index is related to the auroral electrojet and valuable for indicating the occurrence of the substrom (the temporal variation of auroral activity). However, the Fp index senses to the large scale irregularities, which may also influence by convection, the correlation coefficients for Fp and AE thus are not high. Another important characteristic in the figures is that the maximal Fp (the maximal intensity of irregularities) increases with Kp and AE. Referring to Figs. 5 and 7, the percentages of Fp ≥ 50 and Fp ≥ 200 both increases with Kp and AE. The increasing of Kp or AE implies more solar energy transferred into the magnetosphere, which may causes the auroral activity more frequently and intense. This not only creates more severe ionization in the auroral oval but also expands the oval itself. Consequently, the occurrence of irregularities (Fp ≥ 50) and strong irregularities (Fp ≥ 200) both are increasing. Moreover, Fp ≥ 200 is nearly negligible when Kp < 4. This result indicates that, during the solar minimum, there is a threshold for strong irregularities, which almost only occur in the magnetic disturbance period (Kp > 4). Finally, the magnetic indices often have higher values in the E-months (Russell and McPherron 1973). In 2007 and 2008, the mean of Ap (the linear version of Kp) and AE were peaked in the E-months (Fig. 13). Meanwhile, in Figs. 2 and 3, Fp ≥ 50 and Fp ≥ 200 also peaked in the E-months, which corresponds to the above discussions.

4.3 The Variation of TEC Fluctuations and Scintillations

Regarding the irregularities around Tromsø in the nightside sector, Kersley et al. (1988) have reported the occurrences of amplitude and phase scintillations at Kiruna, Sweden during the solar minimum (September 1984 to September 1986). This just mentioned paper showed that the occurrences of the two scintillation types in summer and autumn were higher than that in winter and early spring. Basu et al. (1988) also reported the occurrences of intensity scintillations at Tromsø in the same period (March 1984 to December 1986). This paper showed that, regardless of the magnetic condition, the occurrences were extremely low without a definitive pattern. In the present study, Fp ≥ 50 occurred frequently in all seasons, and Fp ≥ 200 tended to occur in the E-months. These results show that the seasonal variation of irregularities in the three studies are inconsistent, although sites are almost identical and observations all are in the solar minimum.

Before further discussing, it is worth mentioning the principles of scintillations and TEC fluctuations. Scintillations are based on the diffraction of radio waves. When plane waves emit from a satellite and pass through ionospheric irregularities, their phases may become irregular due to diffraction. At the ground receiver, the irregular wave phases combine either constructively or destructively and then cause wave amplitudes increasing or decreasing. These varied phases and amplitudes are indicators for irregularities. On the other hand, TEC fluctuations are based on the

refraction. If the frequency of radio waves is much higher than the ionospheric plasma frequency, plan waves will remain in plan even though they pass through ionospheric irregularities. However, the observed phases at the ground receiver will delay or advance due to refraction. The amount of changing phases can be converted into TEC, and the TEC variation indicates the existence of irregularities (Rino 1979a, b; Yeh and Liu 1982; Engavale and Bhattacharyya 2005; Kintner et al. 2007).

There are factors related to the results of three studies above. First, studies used different satellite systems; therefore, the sampling locations and times were also different. Kersley et al. (1988) used Navy Navigation Satellite System (the predecessor of GPS), which comprises five satellites and thus provides more data than the single HiLat satellite that was used in Basu et al. (1988). Regarding GPS, it has most number of satellites and provides the largest amount of data, which make its result more reliable. The second factor concerns the scale size of irregularities. The Fp index at high latitudes is sensitive to irregularities with the scale size around 60 km. For amplitude scintillations, the scale size is based on the size of the Fresnel zone. Regard to phase scintillations, the scale size depends on the sampling interval and irregularity drift velocity. This size is larger than the Fresnel zone at least, and larger irregularities have more contributions (Yeh and Liu 1982). Kersley et al. (1988) measured scintillations at 150 MHz and Basu et al. (1988) measured at 250 MHz. Thus, the order of scale size from small to large are the intensity scintillations in Basu et al. (1988), the amplitude scintillations in Kersley et al. (1988), the phase scintillations in Kersley et al. (1988), and then the Fp index in this study. At high latitudes, background plasma drift is very fast, which causes the small-scale irregularities eliminating easily and quickly. Thus, the occurrences in Basu et al. (1988) were extremely low. Moreover, the background electron density is important for the scintillation activity, especially in lower frequencies (Yeh and Liu 1982). This may be the reason that the occurrences of scintillations in Kersley et al. (1988) were high in summer.

In addition to the factors concerning instrument and measurement, physical environment also plays a crucial role. Liou et al. (2011) confirmed that the nighttime aurora is more intense in winter or darkness than in summer or sunlight, which is due to the feedback of the ionospheric conductivity resulting from the solar extreme ultraviolet (EUV). Similarly, the occurrences of Fp ≥ 50 in the J-months were also lower than that in the D-months. Furthermore, Basu (1975) has pointed out that the geometry of the magnetotail may influence particle precipitation and then auroral irregularities. Although the results in Kersley et al. (1988) agree with the theory of Basu (1975), many observations do not. Kubyshkina et al. (2015) detailed studied this topic and concluded that the more symmetrical magnetotail accumulates and stores the magnetic flux more effective, and then causes substorms more intense. On the contrary, the bending magnetotail is less stable and breaks after smaller energy input, which causes substroms happening in lower intensity and more frequently. On the basis of this, we can speculate that, in the E-months, the magnetotial is more symmetrical, which results more intense substorms and then stronger irregularities (this is the reason that AE and Fp ≥ 200 both peak in the E-months). In the D- and J-months, the magnetotial is more bending. Substorms are then less intense but occur more frequently. However, the high background electron density (ionospheric conductivity) resulting from the solar EUV in the J-months suppresses the auroral activity. Therefore, irregularity occurrence and duration are higher and longer in the D-months than in the J-months. Finally, we have shown that the maximal Fp and the percentage of Fp ≥ 200 both increase with Kp and AE. In addition, the magnetic indices also peak in the E-months. These suggest that energy transformation between the solar wind and the geomagnetic field is more effective in the E-months, which results the high occurrences of stronger irregularities in the E-months.

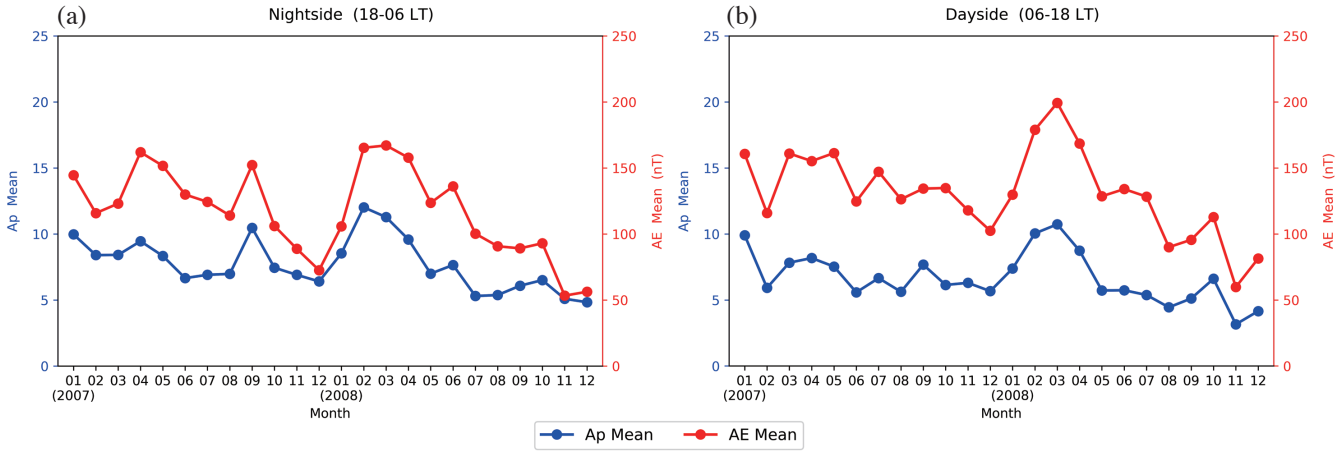

Fig. 13. The meanly mean of Ap and AE for (a) the nightside sector (18 - 06 LT) and (b) the dayside sector (06 - 18 LT). (Color online only)

4.4 TEC Fluctuations and the Heights of Irregularities

The heights of irregularities in the auroral region has been studied for a long time. Some studies reported that irregularities mainly distribute in the F region (Penndorf 1962; Calvert and Schmid 1964; Frihagen and Liszka 1965), others showed that the E region irregularities are important (Basu et al. 1993; Coker et al. 1995), and others suggested that irregularities are in both regions (Pike et al. 1977; Whalen et al. 1977; Aarons and Lin 1999; Aarons et al. 2000). From Figs. 8 and 9, we found that the auroral activity creates the high electron density structure, which involves irregularities and thus activates FROT. With larger thickness of the structure, FROT is also more active. However, the very high electron density structure in a narrow range of heights still can result strong FROT activity. In short, the Fp value can be larger than 50 when the high electron density structure occurs in the E region or extends from the E region to the F region. The results of Figs. 10 and 11 also support this conclusion. In Fig. 10, the density variations distribute in the E and F regions. In Fig. 11, the density variations are in the E region only. To confirm those variations being irregularities, the ionograms from the ionosonde at Tromsø were checked. Figure 14 shows ionograms at 2030 and 2045 UT on 2007-04-24. Both ionograms have spread F and spread E phenomena. Thus, irregularities actually existed in the E and F regions. Figure 15 shows ionograms at 1930 and 1945 UT on 2007-01-15. Because the spread echoes occurred on the E region trace only, irregularities were in the E region.

5. CONCLUSION

This study investigated GPS TEC fluctuations over Tromsø, Norway during 2007 - 2008. Tromsø is located at high latitudes, which is inside the auroral oval during nighttime. The years 2007 and 2008 belong to the low solar activity period, in which the solar minimum is 2008. The TEC fluctuation index Fp that defined by Mendillo et al. (2000) was adopted to quantify TEC fluctuations. This index is sensitive to large scale irregularities at high latitudes. The level $Fp \geq 50$ is used to indicate the existence of irregularities, in which the sub-levels $50 \leq Fp < 200$ and $Fp \geq 200$ represent moderate and strong irregularities, respectively. The investigations include the seasonal and temporal variation of Fp and the correlation between Fp and the magnetic indices Kp and AE. To get the information about the irregularity heights, Fp was also compared with ionospheric electron density observed by the Tromsø UHF ISR and the electron density profile provided by COSMIC. These investigations provide a general picture about large scale irregularities at auroral region during the solar minimum.

The results are summarized as follow: for the nightside sector, $Fp \geq 50$ occurred frequently but the occurrences in the J-months were little lower than that in the D- and E-months; the occurrences of $Fp \geq 200$ peaked in the E-months. For the dayside sector, $Fp \geq 50$ peaked in the E-months; the occurrences of $Fp \geq 200$ were very low without a clear pattern. For the temporal variation, $Fp \geq 50$ mainly occurred in the period 18 - 04 LT, in which the maxima located in the E-months around 22 LT. Moreover, the duration of $Fp \geq 50$ was longest in the E-months but shortest in the J-months, and the starting time of $Fp \geq 50$ in the J-months was behind that in the E- and D-months. For $Fp \geq 200$, it had extremely low occurrences, which mainly distributed in the period 18 - 02 LT in the E-months. Turning to the correlation between Fp and magnetic indices, the linear correlation between Fp and Kp was poor, but that between Fp and AE was moderate. The clear characteristic is that the maximal Fp and the percentages of $Fp \geq 50$ and $Fp \geq 200$ all increased with Kp and AE. Especially, $Fp \geq 200$ is nearly negligible when $Kp < 4$. Finally, the comparisons between Fp and ionospheric electron density showed that Fp was larger than 50 when the high electron density structure located in the E region or extended from the E region to the F region, in which the structure was resulted from the auroral activity and involved irregularities.

From those results, we found that (1) $Fp \geq 50$ at auroral region mainly relates to the auroral activity. (2) The temporal variation of Fp consists with that of scintillations in early studies but the seasonal variation does not. The discrepancy might be caused by different instruments, irregularity scale sizes, and physical environments between the studies. (3) The seasonal variation of Fp can be explained by the effect of sunlight (solar EUV) and the geometry of the magnetotail. (4) The linear correlation between Fp and AE is moderate but that between Fp and Kp is poor. Moreover, occurrence of irregularities and their maximal intensity are increased with Kp and AE. In addition, strong irregularities almost only occur in the magnetic disturbance period. (5) Irregularities distribute only in the E region or in the E and F two regions both have ability to cause $Fp \geq 50$.

Acknowledgements WSC was supported by the grant of Ministry of Science and Technology MOST 105-2811-M-231-001. CCL was supported by the grants MOST 106-2111-M-231-001 and MOST 105-2119-M-231-001. FDC was supported by the grant of Bureau of Standards, Metrology and Inspection, Ministry of Economic Affairs, Taiwan BSMI 105-1403-05-05-01. WLT was supported by the grant of Universiti Kebangsaan Malaysia GGPM-2015-027. The authors would like to thank University of Massachusetts Lowell for the access to DIDBase (http://ulcar.uml.edu/DIDBase/), the worldwide digisonde database. The GPS data are available at the website of International GNSS Service (http://www.igs.org/). The ISR data are available at the website of European Incoherent Scatter Scientific Association (http://www.eiscat.com/). The data of the Kiruna all-sky camera are available at the website of Swedish Institute of

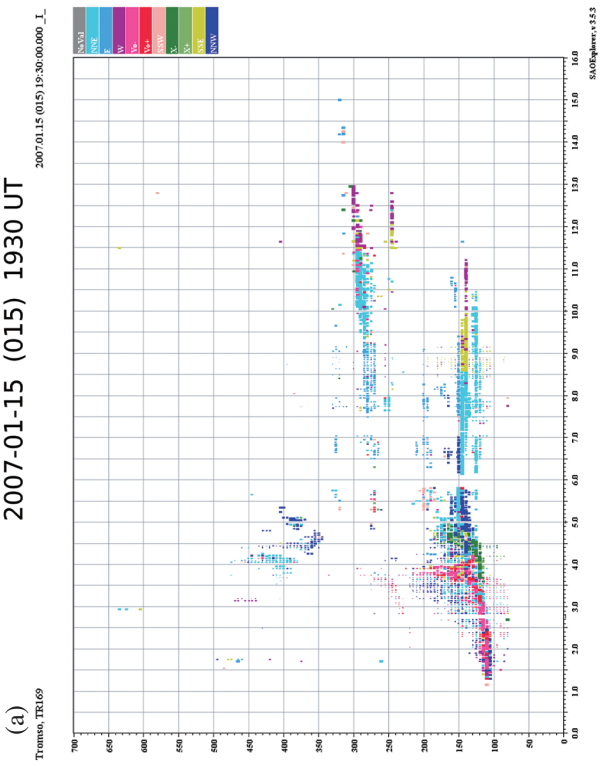

Fig. 15. The ionograms of Tromsø at (a) 1930 UT and (b) 1945 UT on 2007-01-15. (Color online only)

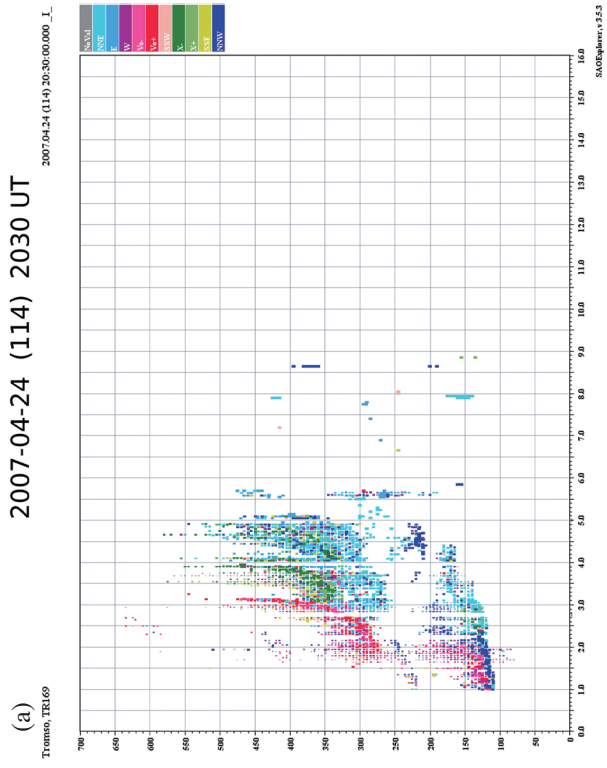

Fig. 14. The ionograms of Tromsø at (a) 2030 UT and (b) 2045 UT on 2007-04-24. (Color online only)

Space Physics (IRF), Kiruna, Swedish (http://www.irf.se/). The Kp and AE data are available at the website of World Data Center for Geomagnetism, Kyoto (http://wdc.kugi.kyoto-u.ac.jp/). The COSMIC data are available at the website of Taiwan Analysis Center for COSMIC (http://tacc.cwb.gov.tw/). The authors would like to thank these organizations for opening their data to the public.

REFERENCES

Aarons, J., 1997: Global positioning system phase fluctuations at auroral latitudes. *J. Geophys. Res.*, **102**, 17219-17231, doi: 10.1029/97JA01118. [Link]

Aarons, J. and B. Lin, 1999: Development of high latitude phase fluctuations during the January 10, April 10-11, and May, 15, 1997 magnetic storms. *J. Atmos. Sol. Terr. Phys.*, **61**, 309-327, doi: 10.1016/S1364-6826-(98)00131-X. [Link]

Aarons, J., M. Mendillo, R. Yantosca, and E. Kudeki, 1996: GPS phase fluctuations in the equatorial region during the MISETA 1994 campaign. *J. Geophys. Res.*, **101**, 26851-26862, doi: 10.1029/96JA00981. [Link]

Aarons, J., B. Lin, M. Mendillo, K. Liou, and M. Codrescu, 2000: Global Positioning System phase fluctuations and ultraviolet images from the Polar satellite. *J. Geophys. Res.*, **105**, 5201-5213, doi: 10.1029/1999JA900409. [Link]

Basu, S., 1975: Universal time seasonal variations of auroral zone magnetic activity and VHF scintillations. *J. Geophys. Res.*, **80**, 4725-4728, doi: 10.1029/JA080i034p04725. [Link]

Basu, S. and J. Aarons, 1980: The morphology of high-latitude VHF scintillation near 70°W. *Radio Sci.*, **15**, 59-70, doi: 10.1029/RS015i001p00059. [Link]

Basu, S., E. MacKenzie, and S. Basu, 1988: Ionospheric constraints on VHF/UHF communications links during solar maximum and minimum periods. *Radio Sci.*, **23**, 363-378, doi: 10.1029/RS023i003p00363. [Link]

Basu, S., S. Basu, R. Eastes, R. E. Huffman, R. E. Daniell, P. K. Chaturvedi, C. E. Valladares, and R. C. Livingston, 1993: Remote sensing of auroral E region plasma structures by radio, radar, and UV techniques at solar minimum. *J. Geophys. Res.*, **98**, 1589-1602, doi: 10.1029/92JA01655. [Link]

Calvert, W. and C. W. Schmid, 1964: Spread-F observations by the Alouette Topside Sounder Satellite. *J. Geophys. Res.*, **69**, 1839-1852, doi: 10.1029/JZ069i009p01839. [Link]

Chen, W. S., C. C. Lee, J. Y. Liu, F. D. Chu, and B. W. Reinisch, 2006: Digisonde spread F and GPS phase fluctuations in the equatorial ionosphere during solar maximum. *J. Geophys. Res.*, **111**, A12305, doi: 10.1029/2006JA011688. [Link]

Chen, W. S., C. C. Lee, F. D. Chu, and S. Y. Su, 2011: Spread F, GPS phase fluctuations, and medium-scale traveling ionospheric disturbances over Wuhan during solar maximum. *J. Atmos. Sol. Terr. Phys.*, **73**, 528-533, doi: 10.1016/j.jastp.2010.11.012. [Link]

Chen, W. S., C. C. Lee, and F. D. Chu, 2016: GPS Phase Fluctuations over Tromsø, Norway in the Low Solar Activity Year, 2016 Taiwan Geosciences Assembly, Taipei, Taiwan.

Chu, F. D., C. C. Lee, W. S. Chen, and J. Y. Liu, 2008: A study of long-term climatology of ionospheric irregularities by using GPS phase fluctuations at the Brazilian longitudes. *Adv. Space Res.*, **41**, 645-649, doi: 10.1016/j.asr.2007.05.003. [Link]

Chu, F. D., W. S. Chen, C. C. Lee, and J. Y. Liu, 2009: A climatological study of nocturnal equatorial F-region irregularities at the west Pacific longitudes by using phase fluctuations of the global positioning system. *J. Atmos. Sol. Terr. Phys.*, **71**, 1441-1449, doi: 10.1016/j.jastp.2008.06.012. [Link]

Coker, C., R. Hunsucker, and G. Lott, 1995: Detection of auroral activity using GPS satellites. *Geophys. Res. Lett.*, **22**, 3259-3262, doi: 10.1029/95GL03091. [Link]

Engavale, B. and A. Bhattacharyya, 2005: Spatial correlation of intensity variations in the ground scintillation pattern produced by equatorial spread-F irregularities. *Indian J. Radio Space Phys.*, **34**, 23-32.

Feldstein, Y. I., 1963: On morphology and auroral and magnetic disturbances at high latitudes. *Geomagn. Aeron.*, **3**, 183-192.

Frihagen, J. and L. Liszka, 1965: A study of auroral zone ionospheric irregularities made simultaneously at Tromsö, Norway and Kiruna Sweden. *J. Atmos. Terr. Phys.*, **27**, 513-523, doi: 10.1016/0021-9169(65)90015-2. [Link]

Hartz, T. R. and N. M. Brice, 1967: The general pattern of auroral particle precipitation. *Planet. Space Sci.*, **15**, 301-329, doi: 10.1016/0032-0633(67)90197-3. [Link]

Hofmann-Wellenhof, B., H. Lichtenegger, and J. Collins, 1997: Global Positioning System: Theory and Practice, Springer-Verlag Wien, New York, USA, 382 pp.

Holzworth, R. H. and C. I. Meng, 1975: Mathematical representation of the auroral oval. *Geophys. Res. Lett.*, **2**, 377-380, doi: 10.1029/GL002i009p00377. [Link]

Hunsucker, R. D. and J. K. Hargreaves, 2003: The High-Latitude Ionosphere and Its Effects On Radio Propagation, Cambridge University Press, Cambridge, U. K., doi: 10.1017/CBO9780511535758. [Link]

Jiao, Y., Y. T. Morton, S. Taylor, and W. Pelgrum, 2013: Characterization of high-latitude ionospheric scintillation of GPS signals. *Radio Sci.*, **48**, 698-708, doi: 10.1002/2013RS005259. [Link]

Kelley, M. C., 1989: The Earth's Ionosphere: Plasma Physics and Electrodynamics, Academic Press, San Francisco, USA, 500 pp.

Kelley, M. C., J. F. Vickrey, C. W. Carlson, and R. Torbert,

1982: On the origin and spatial extent of high-latitude F region irregularities. *J. Geophys. Res.*, **87**, 4469-4475, doi: 10.1029/JA087iA06p04469. [Link]

Kersley, L., S. E. Pryse, and N. S. Wheadon, 1988: Amplitude and phase scintillation at high latitudes over northern Europe. *Radio Sci.*, **23**, 320-330, doi: 10.1029/RS023i003p00320. [Link]

Kersley, L., C. D. Russell, and D. L. Rice, 1995: Phase scintillation and irregularities in the northern polar ionosphere. *Radio Sci.*, **30**, 619-629, doi: 10.1029/94rs03175. [Link]

Keskinen, M. J. and S. L. Ossakow, 1983: Theories of high-latitude ionospheric irregularities: A review. *Radio Sci.*, **18**, 1077-1091, doi: 10.1029/RS018i006p01077. [Link]

Kintner, P. M., B. M. Ledvina, and E. R. de Paula, 2007: GPS and ionospheric scintillations. *Space Weather*, **5**, S09003, doi: 10.1029/2006sw000260. [Link]

Kubyshkina, M., N. Tsyganenko, V. Semenov, D. Kubyshkina, N. Partamies, and E. Gordeev, 2015: Further evidence for the role of magnetotail current shape in substorm initiation. *Earth Planets Space*, **67**, doi: 10.1186/s40623-015-0304-1. [Link]

Lee, C. C., F. D. Chu, W. S. Chen, J. Y. Liu, S. Y. Su, Y. A. Liou, and S. B. Yu, 2009: Spread F, GPS phase fluctuations, and plasma bubbles near the crest of equatorial ionization anomaly during solar maximum. *J. Geophys. Res.*, **114**, A08302, doi: 10.1029/2009JA014195. [Link]

Lei, J., S. Syndergaard, A. G. Burns, S. C. Solomon, W. Wang, Z. Zeng, R. G. Roble, Q. Wu, Y. H. Kuo, J. M. Holt, S. R. Zhang, D. L. Hysell, F. S. Rodrigues, and C. H. Lin, 2007: Comparison of COSMIC ionospheric measurements with ground-based observations and model predictions: Preliminary results. *J. Geophys. Res.*, **112**, A07308, doi: 10.1029/2006JA012240. [Link]

Liou, K., Y. L. Zhang, P. T. Newell, L. J. Paxton, and J. F. Carbary, 2011: TIMED/GUVI observation of solar illumination effect on auroral energy deposition. *J. Geophys. Res.*, **116**, A09305, doi: 10.1029/2010JA016402. [Link]

Mendillo, M., B. Lin, J. Aarons, 2000: The application of GPS observations to equatorial aeronomy. *Radio Sci.*, **35**, 885-904, doi: 10.1029/1999RS002208. [Link]

Penndorf R., 1962: A spread-F index. *J. Atmos. Terr. Phys.*, **24**, 543-545, doi: 10.1016/0021-9169(62)90218-0. [Link]

Pi, X., A. J. Mannucci, U. J. Lindqwister, and C. M. Ho, 1997: Monitoring of global ionospheric irregularities using the Worldwide GPS Network. *Geophys. Res. Lett.*, **24**, 2283-2286, doi: 10.1029/97GL02273. [Link]

Pike, C. P., J. A. Whalen, and J. Buchau, 1977: A 12-hour case study of auroral phenomena in the midnight sector: F layer and 6300-Å measurements. *J. Geophys. Res.*, **82**, 3547-3556, doi: 10.1029/JA082i025p03547. [Link]

Prikryl, P., P. T. Jayachandran, S. C. Mushini, D. Pokhotelov, J. W. MacDougall, E. Donovan, E. Spanswick, and J. P. St. Maurice, 2010: GPS TEC, scintillation and cycle slips observed at high latitudes during solar minimum. *Ann. Geophys.*, **28**, 1307-1316, doi: 10.5194/angeo-28-1307-2010. [Link]

Prikryl, P., P. T. Jayachandran, S. C. Mushini, and R. Chadwick, 2011: Climatology of GPS phase scintillation and HF radar backscatter for the high-latitude ionosphere under solar minimum conditions. *Ann. Geophys.*, **29**, 377-392, doi: 10.5194/angeo-29-377-2011. [Link]

Prikryl, P., P. T. Jayachandran, S. C. Mushini, and I. G. Richardson, 2012: Toward the probabilistic forecasting of high-latitude GPS phase scintillation. *Space Weather*, **10**, S08005, doi: 10.1029/2012SW000800. [Link]

Pryse, S. E., L. Kersley, and C. D. Russell, 1991: Scintillation near the F layer trough over northern Europe. *Radio Sci.*, **26**, 1105-1114, doi: 10.1029/91RS00490. [Link]

Rino, C. L., 1979a: A power law phase screen model for ionospheric scintillation: 1. Weak scatter. *Radio Sci.*, **14**, 1135-1145, doi: 10.1029/RS014i006p01135. [Link]

Rino, C. L., 1979b: A power law phase screen model for ionospheric scintillation: 2. Strong scatter. *Radio Sci.*, **14**, 1147-1155, doi: 10.1029/RS014i006p01147. [Link]

Rino, C. L. and S. Matthews, 1980: On the morphology of auroral zone radio wave scintillation. *J. Geophys. Res.*, **85**, 4139-4151, doi: 10.1029/JA085iA08p04139. [Link]

Rino, C. L., R. C. Livingston, R. T. Tsunoda, R. M. Robinson, J. F. Vickrey, C. Senior, M. D. Cousins, J. Owen, and J. A. Klobuchar, 1983: Recent studies of the structure and morphology of auroral zone F region irregularities. *Radio Sci.*, **18**, 1167-1180, doi: 10.1029/RS018i006p01167. [Link]

Russell, C. T. and R. L. McPherron, 1973: Semiannual variation of geomagnetic activity. *J. Geophys. Res.*, **78**, 92-108, doi: 10.1029/JA078i001p00092. [Link]

Schreiner, W. S., S. V. Sokolovskiy, C. Rocken, and D. C. Hunt, 1999: Analysis and validation of GPS/MET radio occultation data in the ionosphere. *Radio Sci.*, **34**, 949-966, doi: 10.1029/1999RS900034. [Link]

Shagimuratov, I. I., A. Krankowski, I. Ephishov, Yu. Cherniak, P. Wielgosz, and I. Zakharenkova, 2012: High latitude TEC fluctuations and irregularity oval during geomagnetic storms. *Earth Planet Space*, **64**, doi: 10.5047/eps.2011.10.015. [Link]

Tiwari, R., H. J. Strangeways, S. Tiwari, and A. Ahmed, 2013: Investigation of ionospheric irregularities and

scintillation using TEC at high latitude. *Adv. Space Res.*, **52**, 1111-1124, doi: 10.1016/j.asr.2013.06.010. [Link]

Tsunoda, R. T., 1988: High-latitude F region irregularities: A review and synthesis. *Rev. Geophys.*, **26**, 719-760, doi: 10.1029/RG026i004p00719. [Link]

Wanninger, L., 1993: Ionospheric monitoring using IGS data. 1993 Berne IGS Workshop, Berne, Switzerland.

Whalen, J. A., R. A. Wagner, and J. Buchau, 1977: A 12-hour case study of auroral phenomena in the mid-night sector: Oval, polar cap, and continuous auro-ras. *J. Geophys. Res.*, **82**, 3529-3546, doi: 10.1029/JA082i025p03529. [Link]

Yeh, K. C. and C. H. Liu, 1982: Radio wave scintillations in the ionosphere. *Proc. IEEE*, **70**, 324-360, doi: 10.1109/PROC.1982.12313. [Link]